J|A|C|S
ARTICLES

Published on Web 09/09/2010

# Supermolecular-Chromophore-Sensitized Near-Infrared-to-Visible Photon Upconversion

Tanya N. Singh-Rachford,[†,||] Animesh Nayak,[‡,§] Maria L. Muro-Small,[†] Sèbastian Goeb,[†,⊥] Michael J. Therien,[*,§] and Felix N. Castellano[*,†]

*Department of Chemistry and Center for Photochemical Sciences, Bowling Green State University, Bowling Green, Ohio 43403, Department of Chemistry, 231 South 34th Street, University of Pennsylvania, Philadelphia, Pennsylvania 19104, and Department of Chemistry, French Family Science Center, 124 Science Drive, Duke University, Durham, North Carolina 27708*

Received June 23, 2010; E-mail: castell@bgsu.edu; michael.therien@duke.edu

***Abstract:*** Selective near-IR (NIR) excitation (780 nm) of the conjugated supermolecule ruthenium(II) [15-(4′-ethynyl-(2,2′;6′,2″-terpyridinyl))-bis[(5,5′,-10,20-di(2′,6′-bis(3,3-dimethylbutoxy)phenyl)porphinato)zinc(II)]ethyne][4′-pyrrolidin-1-yl-2,2′;6′,2″-terpyridine] bis(hexafluorophosphate) (**$Pyr_1RuPZn_2$**) in solutions containing *N,N*-bis(ethylpropyl)perylene-3,4,9,10-tetracarboxylicdiimide (**PDI**) or tetracene gives rise to a substantial anti-Stokes energy gain (**PDI**, 0.70 eV; tetracene, 0.86 eV). Experimental data clearly demonstrate that this upconverted fluorescence signal is produced via **$Pyr_1RuPZn_2$**-sensitized triplet−triplet annihilation (TTA) photochemistry. The TTA process was confirmed by the quadratic dependence of the integrated **$^1$PDI*** emission centered at 541 nm derived from 780 nm laser excitation. The $T_1 \rightarrow T_n$ excited state absorption decay of **$Pyr_1RuPZn_2$**, monitored at 900 nm as a function of **PDI** concentration, revealed Stern−Volmer and bimolecular quenching constants of 10 048 $M^{-1}$ and $5.9 \times 10^8$ $M^{-1}$ $s^{-1}$, respectively, for the **PDI** triplet sensitization process. The $T_1 \rightarrow T_n$ **PDI** extinction coefficient at 560 nm ($\varepsilon_T = 6.6 \times 10^4$ $M^{-1}$ $cm^{-1}$) was determined through the triplet energy transfer method utilizing anthracene as the donor chromophore. **$^3$PDI*** transient triplet absorption dynamics observed as a function of 485 nm incident nanosecond pump laser fluence demonstrate a bimolecular **$^3$PDI***−**$^3$PDI*** TTA rate constant ($k_{TT} = 1.0 \pm 0.2 \times 10^9$ $M^{-1}$ $s^{-1}$). The maximum quantum yield of the supermolecule-sensitized **PDI** upconverted emission ($\Phi_{UC} = 0.0075 \pm 0.0002$) was determined relative to $[Os(phen)_3][PF_6]_2$ at an incident laser power of 22 mW at 780 nm. This study successfully demonstrates NIR-to-visible photon upconversion and achieves a new record anti-Stokes shift of 0.86 eV for sensitized TTA, using the supermolecular **$Pyr_1RuPZn_2$**sensitizer. The stability of the **$Pyr_1RuPZn_2$**/**PDI** chromophore combination is readily apparent as continuous irradiation at 780 nm produces 541 nm centered fluorescence with no significant decrease in intensity measured over time domains exceeding several hours. The molecular components of these NIR-to-vis upconverting compositions illustrate that substantial anti-Stokes energy gains via a TTA process can be effortlessly realized.

## Introduction

Photon upconversion based on sensitized triplet−triplet annihilation (TTA) continues to emerge as a promising low-power initiated wavelength-shifting technology. In the generic TTA scheme, photon upconversion is facilitated by selective excitation of strongly absorbing sensitizer chromophores that both rapidly and efficiently internally convert to the long-lived lowest energy triplet excited state. Triplet−triplet energy transfer then ensues to select molecular species energetically poised for TTA and the desired annihilation-producing fluorescence. This strategy has proven exceedingly effective when late-transition-metal-based sensitizers are combined in concert with a variety of organic-based triplet acceptors/annihilators.[1−20] In many recent examples, the efficiency of sensitized TTA-based up-

[†] Bowling Green State University.
[‡] University of Pennsylvania.
[§] Duke University.
[||] Current address: The Dow Chemical Company, Analytical Sciences, 1897 Building, Midland, Michigan 48667, USA.
[⊥] Current address: Université d'Angers, CIMA UMR CNRS 6200-UFR Sciences, 2 Boulevard Lavoisier, 49045, Angers, France.

(1) Kozlov, D. V.; Castellano, F. N. *Chem. Commun.* **2004**, 2860–2861.
(2) Islangulov, R. R.; Castellano, F. N. *Angew. Chem., Int. Ed.* **2006**, *45*, 5957–5959.
(3) Islangulov, R. R.; Kozlov, D. V.; Castellano, F. N. *Chem. Commun.* **2005**, 3776–3778.
(4) Zhao, W.; Castellano, F. N. *J. Phys. Chem. A* **2006**, *110*, 11440–11445.
(5) Islangulov, R. R.; Lott, J.; Weder, C.; Castellano, F. N. *J. Am. Chem. Soc.* **2007**, *129*, 12652–12653.
(6) Singh-Rachford, T. N.; Islangulov, R. R.; Castellano, F. N. *J. Phys. Chem. A* **2008**, *112*, 3906–3910.
(7) Singh-Rachford, T. N.; Haefele, A.; Ziessel, R.; Castellano, F. N. *J. Am. Chem. Soc.* **2008**, *130*, 16164–16165.
(8) Singh-Rachford, T. N.; Castellano, F. N. *J. Phys. Chem. A* **2008**, *112*, 3550–3556.
(9) Singh-Rachford, T. N.; Castellano, F. N. *Inorg. Chem.* **2009**, *48*, 2541–2548.
(10) Singh-Rachford, T. N.; Lott, J.; Weder, C.; Castellano, F. N. *J. Am. Chem. Soc.* **2009**, *131*, 12007–12014.
(11) Singh-Rachford, T. N.; Castellano, F. N. *J. Phys. Chem. Lett.* **2010**, *1*, 195–200.

  

conversion has reached the point where the process is easily visualized by the unassisted eye in the laboratory.[3,5,7−11,20,21]

Efficiently functioning upconversion systems based on sensitized TTA generally possess energy gaps of ∼0.5 eV between the excitation light and the maximum singlet fluorescence emission band exhibited by the acceptor/annihilator.[22] One facet of research in this area has focused attention on the measurement and improvement of quantum efficiencies in these light conversion processes. Of vital importance are newly emergent data clearly demonstrating that sensitized TTA upconversion quantum efficiencies do indeed surpass the 11.1% spin statistical limit imposed by the assumption that, subsequent to TTA, only the singlet-excited encounter complex produces singlet emitting molecules.[22,23] Considering that two separate published reports reveal upconversion efficiencies of 15.1% and 16% in distinct solution-based compositions,[22,23] it becomes clear that the sensitized triplet excited states leading to TTA can be recycled, eventually producing more upconverted singlet fluorescence. These results, coupled with the fact that select solid state upconversion materials display significant performance improvements with increasing temperature,[5,10] strongly suggest the viability of translating this technology to real-world applications. In addition to quantum efficiency improvements, many investigations have focused on generalizing this phenomenon across energetically relevant triplet sensitizers and acceptor/annihilators resulting in anti-Stokes shifts spanning the visible (420−600 nm) and near-visible (360−420 nm) regions of the spectrum.[1−22] Most recently, we reported an upconverting composition that offers the largest anti-Stokes energy difference experimentally realized to date (0.80 eV).[11] Through the use of simultaneous two-photon excitation ($\lambda_{ex}$ = 860 nm) in this system, we were also able to "artificially" generate a marked anti-Stokes shift of 1.38 eV, which exhibited a quartic ($x^4$) incident light power dependence for sensitized TTA.[24] To truly harness the full potential of upconversion technology for possible device applications, new chromophore combinations must be evaluated in order to further extend wavelength shifting capabilities from near-IR (NIR) sensitizers and to enhance upconversion quantum yields. These goals in part inspire the present contribution, wherein we not only successfully demonstrate NIR-to-visible photon upconversion but also achieve a new record anti-Stokes shift of 0.86 eV for sensitized TTA using a supermolecular chromophore triplet sensitizer.[25−32]

In terms of NIR-to-visible upconversion, one of the most difficult metrics involves identifying NIR absorbing sensitizers that possess appreciable excited state lifetimes ($\tau_T > \mu s$) along with sufficient triplet state energies that are appropriately poised for exothermic energy transfer to the acceptor/annihilator. NIR-to-vis upconversion via TTA requires highly soluble acceptor/annihilator chromophores that not only have excited state energies that are amenable to NIR sensitization but also provide anti-Stokes wavelength shifts of sufficient magnitude to generate visible emission and a resultant annihilation-based electronically excited singlet state that manifests high quantum yield fluorescence, in order to afford light production at a chromophore concentration that is viable for device applications.

In the present contribution, we simultaneously address all of these chromophore-limiting issues and delineate archetypal molecular components that provide NIR-to-vis upconversion via a triplet−triplet annihilation process. Importantly, this work defines a new genre of NIR absorbing supermolecular chromophores that can function as sensitizers in light-producing upconversion schemes that drive substantial anti-Stokes energy gain. These nonemissive superchromophores feature (porphinato)zinc(II) (PZn) and metal(II)polypyridyl (M) units connected via an ethynyl linker that mixes effectively PZn-based and metal polypyridyl charge-resonance absorption oscillator strength, giving rise to (i) extensive excited state M-PZn interpigment electronic interactions, (ii) high oscillator NIR absorption manifolds, and (iii) low-lying excited states that feature highly polarized charge-separated character that manifest long ($\mu s$) excited-triplet lifetimes.[25−32] We show that a representative MPZn chromophore, used in concert with a high singlet fluorescence quantum yield perylenediimide (**PDI**) dye,[33,34] provides upconverted visible fluorescence centered at 541 nm under experimental conditions that exploit a 780 nm incident laser irradiation wavelength. This work evaluates all the dynamical processes associated with the observed upconversion process, determines the TTA rate constant ($k_{TT}$) for **PDI**-based annihilation, and discusses relevant chromophore attributes


(12) Baluschev, S.; Jacob, J.; Avlasevich, Y. S.; Keivanidis, P. E.; Miteva, T.; Yasuda, A.; Nelles, G.; Grimsdale, A. C.; Muellen, K.; Wegner, G. *ChemPhysChem* **2005**, *6*, 1250–1253.
(13) Baluschev, S.; Keivanidis, P. E.; Wegner, G.; Jacob, J.; Grimsdale, A. C.; Muellen, K.; Miteva, T.; Yasuda, A.; Nelles, G. *Appl. Phys. Lett.* **2005**, *86*, 061904/1–061904/3.
(14) Baluschev, S.; Miteva, T.; Yakutkin, V.; Nelles, G.; Yasuda, A.; Wegner, G. *Phys. Rev. Lett.* **2006**, *97*, 143903(1)–143903(3).
(15) Baluschev, S.; Yakutkin, V.; Miteva, T.; Avlasevich, Y.; Chernov, S.; Aleshchenkov, S.; Nelles, G.; Cheprakov, A.; Yasuda, A.; Muellen, K.; Wegner, G. *Angew. Chem., Int. Ed.* **2007**, *46*, 7693–7696.
(16) Baluschev, S.; Yakutkin, V.; Wegner, G.; Miteva, T.; Nelles, G.; Yasuda, A.; Chernov, S.; Aleshchenkov, S.; Cheprakov, A. *Appl. Phys. Lett.* **2007**, *90*, 181103/1–181103/3.
(17) Monguzzi, A.; Mezyk, J.; Scotognella, F.; Tubino, R.; Meinardi, F. *Phys. Rev. B* **2008**, *78*, 195112/1–195112/5.
(18) Monguzzi, A.; Tubino, R.; Meinardi, F. *J. Phys. Chem. A* **2009**, *113*, 1171–1174.
(19) Merkel, P. B.; Dinnocenzo, J. P. *J. Lumin.* **2009**, *129*, 303–306.
(20) Miteva, T.; Vladimir, Y.; Nelles, G.; Baluschev, S. *New J. Phys.* **2008**, *10*, 103002.
(21) Singh-Rachford, T. N.; Castellano, F. N. *J. Phys. Chem. A* **2009**, *113*, 5912–5917.
(22) Singh-Rachford, T. N.; Castellano, F. N. *Coord. Chem. Rev.* **2010**, *254*, 2560–2573.
(23) Cheng, Y. Y.; Khoury, T.; Clady, R. G. C. R.; Tayebjee, M. J. R.; Ekins-Daukes, N. J.; Crossley, M. J.; Schmidt, T. W. *Phys. Chem. Chem. Phys.* **2010**, *12*, 66–71.
(24) Singh-Rachford, T. N.; Castellano, F. N. *J. Phys. Chem. A* **2009**, *113*, 9266–9269.
(25) Uyeda, H. T.; Zhao, Y.; Wostyn, K.; Asselberghs, I.; Clays, K.; Persoons, A.; Therien, M. J. *J. Am. Chem. Soc.* **2002**, *124*, 13806–13813.
(26) Duncan, T. V.; Rubtsov, I. V.; Uyeda, H. T.; Therien, M. J. *J. Am. Chem. Soc.* **2004**, *126*, 9474–9475.
(27) Xu, T.; Wu, S. P.; Miloradovic, I.; Therien, M. J. *Nano Lett.* **2006**, *6*, 2387–2394.
(28) Strzalka, J.; Xu, T.; Tronin, A.; Wu, S. P.; Miloradovic, I.; Kuzmenko, I.; Gog, T.; Therien, M. J.; Blasie, J. K. *Nano Lett.* **2006**, *6*, 2395–2405.
(29) Duncan, T. V.; Ishizuka, T.; Therien, M. J. *J. Am. Chem. Soc.* **2007**, *129*, 9691–9703.
(30) Keinan, S.; Therien, M. J.; Beratan, D. N.; Yang, W. *J. Phys. Chem. A* **2008**, *112*, 12203–12207.
(31) Duncan, T. V.; Song, K.; Hung, S.-T.; Miloradovic, I.; Nayak, A.; Persoons, A.; Verbiest, T.; Therien, M. J.; Clays, K. *Angew. Chem., Int. Ed.* **2008**, *47*, 2978–2981.
(32) Hu, X.; Xiao, D.; Keinan, S.; Asselberghs, I.; Therien, M. J.; Clays, K.; Yang, W.; Beratan, D. N. *J. Phys. Chem. C* **2010**, *114*, 2349–2359.
(33) Wurthner, F. *Chem. Commun.* **2004**, 1564–1579.
(34) Wasielewski, M. R. *J. Org. Chem.* **2006**, 5051–5066.

responsible for the observations in the present photochemical upconversion process.

## Experimental Section

**General.** Ruthenium(II) [15-(4′-ethynyl-(2,2′;6′,2″-terpyridinyl))-bis[(5,5′,-10,20-di(2′,6′-bis(3,3-dimethylbutoxy)phenyl)porphinato)zinc(II)]ethyne][4′-pyrrolidin-1-yl-2,2′;6′,2″-terpyridine] bis(hexafluorophosphate) (**Pyr$_1$RuPZn$_2$**)[29] and *N*,*N*-bis(ethylpropyl)-perylene-3,4,9,10-tetracarboxylicdiimide (**PDI**)[35] were prepared according to published procedures. $[Os(phen)_3](PF_6)_2$ was synthesized according to a modified literature procedure,[36] using $K_2OsCl_6$ (Aldrich Chemical Co.) as the starting material in ethylene glycol in a microwave synthesis (CEM Discover) at 214 °C for 20 min at atmospheric pressure. Spectroscopic grade 2-methyltetrahydrofuran (MTHF) was purchased from Aldrich Chemical Co. and used as received.

**Spectroscopic Measurements.** Static absorption spectra were measured with a Cary 50 Bio UV−vis spectrophotometer (Varian). Steady-state photoluminescence spectra were acquired using either a PTI single photon counting spectrofluorimeter or a time-correlated single photon counting (TCSPC) spectrometer (Edinburgh Instruments, LifeSpec II). The emission from the latter was measured using a microchannel plate photomultiplier tube (Hamamatsu R3809U-50) in a Peltier-cooled housing. A Ti:Sapphire laser (Chameleon Ultra II, Coherent) was utilized as the excitation light source (provided 780 nm, 80 MHz) for all static measurements. The incident laser power was varied using a series of neutral density filters placed in front of the sample. Laser power was monitored using a Molectron Power Max 5200 power meter. For fluorescence intensity decay measurements, the Chameleon laser was tuned to 950 nm, pulse picked to a 4 MHz repetition rate (Coherent 9200 Pulse Picker), and finally frequency doubled (APE-GmbH SHG Unit) to afford sample excitation, $\lambda_{ex} = 475$ nm. The TCSPC fluorescence intensity decays were analyzed using Edinburgh FAST software. The triplet lifetime of **Pyr$_1$RuPZn$_2$** was determined using transient absorption flash photolysis with specific instrumentation described below. All luminescence samples were prepared either in a 1 cm quartz cell purchased from Starna Cells or in a specially designed 1 cm optical cell with a 3.5 mL nominal volume bearing a side arm round-bottom flask and were degassed for 30 min with high purity argon or subjected to a minimum of three freeze−pump−thaw degas cycles prior to all measurements.

**Quantum Yield Measurements.** The prompt fluorescence quantum yield of **PDI** in MTHF was measured relative to rhodamine B in ethanol, $\Phi_{std} = 0.49$ at $\lambda_{exc} = 500$ nm[37,38] according to eq 1. The sensitized upconverted fluorescence quantum yield measurements of **PDI** in MTHF were measured relative to $[Os(phen)_3](PF_6)_2$ in acetonitrile using 680 nm excitation at an incident laser power of 22 mW in the optically dilute regime (eq 1). In eq 1,[39] $\Phi_{unk}$, $A_{unk}$, $I_{unk}$, and $\eta_{unk}$ represent the quantum yield, absorbance, integrated photoluminescence intensity, and refractive index of the sample. The corresponding terms for the subscript *std* are for the reference quantum counter, rhodamine B, or $[Os(phen)_3](PF_6)_2$; the quantum yield for the latter under the conditions reported is $\Phi_{std} = 0.021$.[40] Equation 1 incorporates an additional multiplicative factor of 2 since the absorption of two photons is required for the observation of one upconverted photon (in the emission actinometer this ratio is 1 to 1), thereby guaranteeing a maximum conversion efficiency of unity.[22]

$$\Phi_{unk} = 2\Phi_{std}\left(\frac{A_{std}}{A_{unk}}\right)\left(\frac{I_{unk}}{I_{std}}\right)\left(\frac{\eta_{unk}}{\eta_{std}}\right)^2 \quad (1)$$

The integrated intensity of the upconverted fluorescence for **PDI** was analyzed over the 450−670 nm spectral region, whereas that of $[Os(phen)_3](PF_6)_2$ was analyzed over the 600−900 nm wavelength range. All measurements were made under identical experimental conditions, and optically matched solutions at the excitation wavelength were used for both the standard and the sample. Quantum yield values reported herein represent an average of at least two independent measurements. Even though the emission profile of the standard sample does not overlap the upconverted photoluminescence evident at shorter wavelengths, note that the experimentally determined quantum yields were reproducible using this relative actinometric method.

**Laser Flash Photolysis.** Nanosecond transient absorption measurements were made using a Proteus spectrometer (Ultrafast Systems LLC) equipped with a 150 W Xe-arc lamp (Newport), a Chromex monochromator (Bruker Optics), appropriate diffraction gratings for visible and NIR dispersion, and Si or InGaAs photodiode detectors (DET 10A and DET 10C, Thorlabs) optically coupled to the exit slit of the monochromator. Excitation of the samples was achieved using a computer-controlled Nd:YAG laser/OPO system (Opotek, Vibrant LD 355 II) operating at 10 Hz. Single wavelength kinetic data were processed separately in Origin 8.0 with the goodness-of-fit established through visual inspection of the residuals. The triplet−triplet annihilation rate constant (TTA) was calculated by fitting the transient absorption decay of the **PDI** triplet at 560 nm as a function of the incident laser fluence according to eq 2.

$$\frac{d[^3M^*]}{dt} = -k_T[^3M^*] - k_{TT}[^3M^*]^2 \quad (2)$$

Here $[^3M^*]$ is the concentration of the triplet excited state of **PDI**, $k_{TT}$ is the triplet−triplet annihilation rate constant, and $k_T$ is the first-order triplet decay rate constant. Integration of eq 2 provides eq 3 which readily translates into a convenient three-parameter expression (eq 4) that was used to fit the experimental data, minimized by nonlinear least-squares in Origin 8.0.

$$[^3M^*] = \frac{[^3M^*]_0 e^{-k_T t}}{1 + [^3M^*]_0 \frac{k_{TT}}{k_T}(1 - e^{-k_T t})} \quad (3)$$

$$y = \frac{p1}{1 + \left(\frac{p1 \cdot p2}{p3}\right)\exp(p3 \cdot x) - \left(\frac{p1 \cdot p2}{p3}\right)} \quad (4)$$

The terms of eq 4 are defined as $y = [^3M^*]$, $x = t$ (time), $p1 = [^3M^*]_0$, $p2 = k_{TT}$, and $p3 = -k_T$. It should be noted that the measured decay curve for $[^3M^*]$ is in absorbance units; hence to convert this to molar concentration, the triplet excited state extinction coefficient of **PDI** is required. This was determined in this manuscript using the energy transfer method described below [$\varepsilon_T$(**PDI**, 560 nm) = $6.58 \times 10^4$ $M^{-1}$ $cm^{-1}$].

**Triplet Extinction Coefficient.** The molar extinction coefficient of the triplet excited state of **PDI** was determined using the energy transfer method as previously described.[9,41,42] This procedure was selected as the more common singlet depletion method was precluded by the lack of a significant ground state bleach from **PDI** following a nanosecond laser flash (vide infra). The energy transfer method in laser flash photolysis involves the utilization of a donor

(35) Demmig, S.; Langhals, H. *Chem. Ber.* **1988**, *121*, 225–230.
(36) Demadis, K. D.; Dattelbaum, D. M.; Kober, E. M.; Concepcion, J. J.; Paul, J. J.; Meyer, T. J.; White, P. S. *Inorg. Chim. Acta* **2007**, 1143–1153.
(37) Casey, K. G.; Quitevis, E. L. *J. Phys. Chem.* **1988**, *92*, 6590–6594.
(38) Washburn, E. W.; West, C. J.; Dorsey, N. E.; Ring, M. D. *International Critical Tables of Numerical Data. Physics, Chemistry, and Technology*; McGraw-Hill: 1930; Vol. 7.
(39) Demas, J. N.; Crosby, G. A. *J. Phys. Chem.* **1971**, *75*, 991–1024.
(40) Kober, E. M.; Casper, J. V.; Lumpkin, R. S.; Meyer, T. J. *J. Phys. Chem.* **1986**, *90*, 3722–3734.
(41) Carmichael, I.; Hug, G. L. *J. Phys. Chem. Ref. Data* **1986**, *15*, 1–250.
(42) Bensasson, R.; Land, E. J. *Trans. Faraday Soc.* **1971**, *67*, 1904–1915.

***Chart 1.*** Chemical Structures of (a) **$Pyr_1RuPZn_2$** and (b) **PDI**

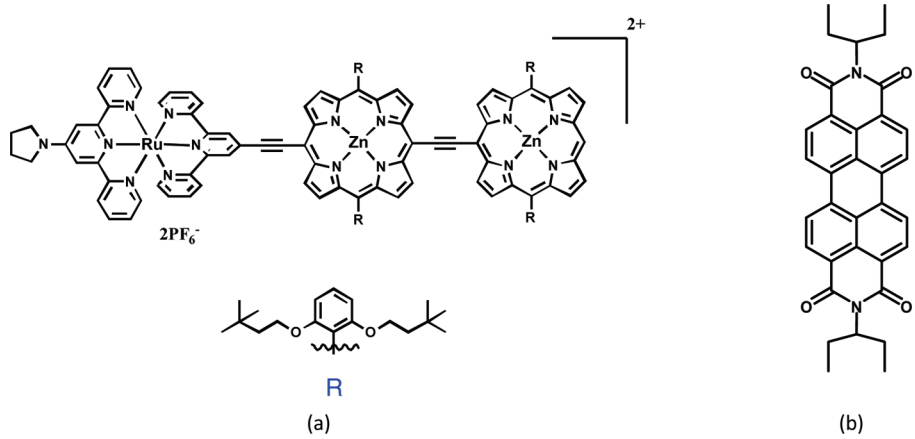


with a known triplet extinction coefficient in the presence of the acceptor. The transient absorption difference spectrum of the donor (prompt signal) and the sensitized acceptor (peak value following energy transfer) are measured at their respective (well separated) wavelength maxima and compared using eq 5. Equation 5 correlates the two molar extinction coefficients, where $^3\varepsilon$(D) and $^3\varepsilon$(A) are the triplet molar extinction coefficients of the donor (known) and acceptor (unknown), respectively. $\Delta A$(D) is the maximum change in optical density of the donor triplet in the absence of the acceptor, and $\Delta A$(A) is the maximum change in optical density of the acceptor triplet when both donor and acceptor are present.

$$\frac{^3\varepsilon(A)}{^3\varepsilon(D)} = \frac{\Delta A(\mathrm{A})}{\Delta A(\mathrm{D})} \qquad (5)$$

In the current experiment, the donor molecule selected was anthracene ($\varepsilon_T$(420 nm) = 42 000 $M^{-1}$ $cm^{-1}$)[41−43] which was excited at 355 nm, well outside the strong ground state **PDI** visible absorbance region.[44] It should be noted that the $T_1 \rightarrow T_n$ transient absorption spectra of anthracene were collected in benzene and MTHF (Figure S1); note that the wavelengths of the difference spectra maxima are solvent dependent. In order to correct for these wavelength shifts, the triplet excited state decay profiles of optically matched solutions of anthracene at the excitation wavelength ($\lambda_{ex}$ = 355 nm) were collected in both solvents at 420 nm. A comparison of the maximum optical density of anthracene obtained at 420 nm in MTHF was made to that obtained in benzene resulting in a ratio of 0.78; this factor was applied to reveal the triplet extinction coefficient of anthracene in MTHF. The triplet excited state extinction coefficient of **PDI** was then calculated for the longest wavelength $T_1 \rightarrow T_n$ absorption feature ($\varepsilon_T$(560 nm) = 6.58 × $10^4$ $M^{-1}$ $cm^{-1}$) and used to determine the $k_{TT}$ value reported below.

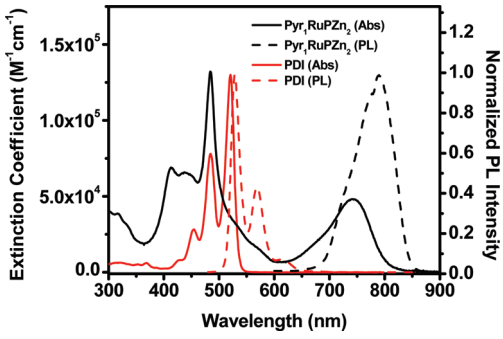


***Figure 1.*** Absorption (showing extinction coefficients) and normalized emission spectra of **$Pyr_1RuPZn_2$** (sensitizer; $\lambda_{ex}$ = 462 nm) and **PDI** (acceptor/annihilator; $\lambda_{ex}$ = 475 nm) in MTHF.

This longer wavelength feature was used exclusively for rate constant determinations as the major transient absorption feature (520 nm) completely overlaps the singlet ground state absorptions, necessitating large corrections for strong ground state bleaching. We consider the substantive overlap of the $S_0 \rightarrow S_n$ transitions with the highest energy $T_1 \rightarrow T_n$ absorption to be unusual, as related work examining Pt(II)-PDI acetylides shows that these bands are well separated in energy.[45,46]

## Results and Discussion

The chemical structures of the compounds investigated in the present study are shown in Chart 1. Figure 1 presents the absorption and emission spectra of the sensitizer, ruthenium(II) [15-(4′-ethynyl-(2,2′;6′,2″-terpyridinyl))-bis[(5,5′,-10,20-di(2′,6′-bis(3,3-dimethylbutoxy)phenyl)porphinato)zinc(II)]ethyne][4′-pyrrolidin-1-yl-2,2′;6′,2″-terpyridine] bis(hexafluorophosphate) (**$Pyr_1RuPZn_2$**), and the acceptor/annihilator, **PDI**, in MTHF solvent. The design, synthesis, spectroscopy, and excited-state dynamics of the chromophore, **$Pyr_1RuPZn_2$**, have previously been described.[29] **$Pyr_1RuPZn_2$** features a meso-to-meso ethyne-bridged bis[(porphinato)zinc(II)] structural unit (**$PZn_2$**);[47−65] a porphyrin *meso*-carbon-to-terpyridyl-4′-carbon ethynyl linkage

(43) Kavarnos, G. J.; Turro, N. J. *Chem. Rev.* **1986**, *86*, 401–449.
(44) Ford, W. E.; Kamat, P. V. *J. Phys. Chem.* **1987**, *91*, 6373–6380.
(45) Rachford, A. A.; Goeb, S.; Castellano, F. N. *J. Am. Chem. Soc.* **2008**, *130*, 2766–2767.
(46) Danilov, E. O.; Rachford, A. A.; Goeb, S.; Castellano, F. N. *J. Phys. Chem. A* **2009**, *113*, 5763–5768.
(47) Lin, V. S.-Y.; DiMagno, S. G.; Therien, M. J. *Science* **1994**, *264*, 1105–1111.
(48) Lin, V. S.-Y.; Therien, M. J. *Chem.—Eur. J.* **1995**, *1*, 645–651.
(49) Angiolillo, P. J.; Lin, V. S.-Y.; Vanderkooi, J. M.; Therien, M. J. *J. Am. Chem. Soc.* **1995**, *117*, 12514–12527.
(50) Kumble, R.; Palese, S.; Lin, V. S.-Y.; Therien, M. J. *J. Am. Chem. Soc.* **1998**, *120*, 11489–11498.
(51) Shediac, R.; Gray, M. H. B.; Uyeda, H. T.; Johnson, R. C.; Hupp, J. T.; Angiolillo, P. J.; Therien, M. J. *J. Am. Chem. Soc.* **2000**, *122*, 7017–7033.
(52) Angiolillo, P. J.; Susumu, K.; Uyeda, H. T.; Lin, V. S.-Y.; Shediac, R.; Therien, M. J. *Synth. Met.* **2001**, *116*, 247–253.
(53) Fletcher, J. T.; Therien, M. J. *J. Am. Chem. Soc.* **2002**, *124*, 4298–4311.
(54) Fletcher, J. T.; Therien, M. J. *Inorg. Chem.* **2002**, *41*, 331–341.
(55) Susumu, K.; Therien, M. J. *J. Am. Chem. Soc.* **2002**, *124*, 8550–8552.
(56) Rubtsov, I. V.; Susumu, K.; Rubtsov, G. I.; Therien, M. J. *J. Am. Chem. Soc.* **2003**, *125*, 2687–2696.
(57) Angiolillo, P. J.; Uyeda, H. T.; Duncan, T. V.; Therien, M. J. *J. Phys. Chem. B* **2004**, *108*, 11893–11903.
(58) Ghoroghchian, P. P.; Frail, P. R.; Susumu, K.; Blessington, D.; Brannan, A. K.; Bates, F. S.; Chance, B.; Hammer, D. A.; Therien, M. J. *Proc. Natl. Acad. Sci. U.S.A.* **2005**, *102*, 2922–2927.

***Scheme 1.*** Qualitative Energy Level Diagram of the Sensitized Triplet−Triplet Annihilation Process between **$Pyr_1RuPZn_2$** and **PDI**

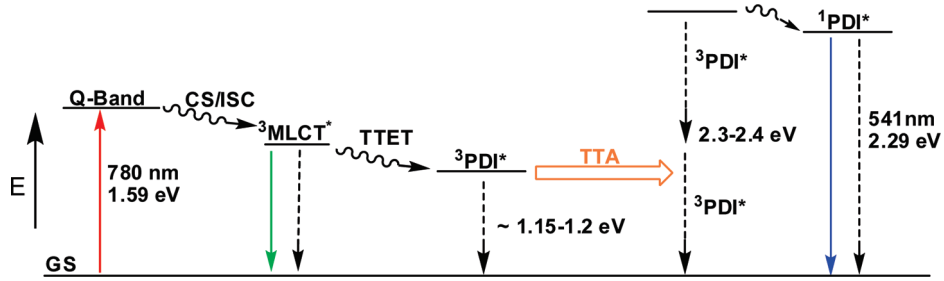


topology conjugates a (terpyridyl)$_2$ruthenium(II) moiety to this structure, which bears an electron-releasing 4′-pyrrolidinyl (Pyr) substituent on its terminal terpyridine ligand (**$Pyr_1Ru$**).[29] The nature of chromophore-to-chromophore connectivity in **$Pyr_1RuPZn_2$** mixes effectively PZn $\pi-\pi^*$ and metal polypyridyl-based charge-resonance absorption oscillator strength and aligns the respective charge transfer (CT) transition dipoles of these building blocks along the highly conjugated molecular axis. These structures manifest substantial interpigment electronic interactions, intensely absorbing broad transitions that extend deep into the NIR region of the spectrum, extensive excited-state electronic delocalization, a manifold of low-lying $T_1$ states having significant charge-separated character, high oscillator strength triplet $T_1 \rightarrow T_n$ transitions, and $\mu$s time-scale excited triplet state relaxation dynamics.[25−32] The combination of these photophysical properties make this supermolecular chromophore based on **$Pyr_1Ru$** and **$PZn_2$** building blocks an attractive sensitizer for use in a NIR upconverting scheme.[25−32,47−65]

The fluorescence spectrum of **$Pyr_1RuPZn_2$** in MTHF is shown in Figure 1; low temperature emission spectra (77 K) illustrate that the NIR fluorescence ($S_1 \rightarrow S_0$) originates from an excited state dominated by (porphyrin-ethyne)$_2$-terpyridine $^1\pi-\pi^*$ ($Q_x$) character (Figure S2).[29] Note that no **$Pyr_1RuPZn_2$** phosphorescence is observed in MTHF containing 10% ethyliodide at 77 K; its triplet excited state lifetime (determined via transient absorption studies, vide infra) in deaerated MTHF corresponds to 17.2 $\mu$s at ambient temperature.

The acceptor/annihilator, **PDI**, is attractive for use in an upconverting scheme since it is known to exhibit exceptional chemical, thermal, and photochemical stability, in addition to large absorptive extinction coefficients and a substantial singlet fluorescence quantum yield.[66−69] **PDI** possesses high oscillator strength absorption bands in the visible region of the spectrum with wavelength maxima at 453 nm ($\varepsilon = 2.82 \times 10^4$ M$^{-1}$ cm$^{-1}$), 485 nm ($\varepsilon = 7.79 \times 10^4$ M$^{-1}$ cm$^{-1}$), and 521 nm ($\varepsilon = 1.30 \times 10^5$ M$^{-1}$ cm$^{-1}$); see Figure 1. The fluorescence spectrum of **PDI** displays almost perfect mirror image symmetry with the absorption spectrum with wavelength maxima at 528, 568, and 616 nm. PDI possesses a fluorescence quantum yield of 0.78; and a singlet excited state lifetime of 4.35 ns [determined by TCSPC ($\lambda_{ex} = 475$ nm), Figure S3]. While the triplet excited state energy of **PDI** could not be determined on an absolute basis, it is estimated to be between 1.15 and 1.2 eV based on excited-state dynamical measurements (vide infra, Scheme 1). No **PDI** phosphorescence is observed in MTHF containing 10% ethyliodide at 77 K, indicating that the quantum yield for this process is indubitably low. It should be noted that the triplet energy of a structurally related **PDI** derivative has previously been estimated to lie between 1.14 and 1.2 eV,[44] which is in good agreement with that proposed for the **PDI** derivative in the present study.

Since it was not possible to observe the steady state phosphorescence of **$Pyr_1RuPZn_2$** in MTHF, nanosecond laser flash photolysis was utilized to measure the Stern−Volmer ($K_{sv}$) and bimolecular ($k_q$) quenching constants for **$Pyr_1RuPZn_2$** deactivation by **PDI**. The $K_{sv}$ and $k_q$ values provide an indication of the exothermicity of the triplet energy transfer between **$Pyr_1RuPZn_2$** and **PDI**. Figure 2a shows the nanosecond transient absorption difference spectrum of 7.0 $\mu$M **$Pyr_1RuPZn_2$** measured at several delay times in deaerated MTHF upon excitation (1.0 mJ/pulse) at 700 nm. Negative transient signals are observed between 368−498 nm and 635−797 nm corresponding to ground state bleaching of the extensively mixed transitions that trace their genesis to the porphyrin B and Q and the polypyridyl metal MLCT states.[29] Broad positive excited triplet state absorptions are observed between 498−635 and 797 nm to 1400 nm (Figure 2a). Note that in the microsecond time domain the amplitudes of the excited state transient signals in the TA-difference spectra acquired over the 350−800 nm spectral regime are about five times less than that observed over the 800−1400 nm spectral window, in contrast to analogous data obtained over the fs−ns time domain.[29] Analysis of the absorption transient signals at 480 and 1100 nm yielded identical single exponential decay kinetics (17.2 $\mu$s). Nanosecond transient absorption difference spectra for 4.2 $\mu$M **PDI** (the acceptor/annihilator) were also measured at several delay times in deaerated MTHF (485 nm excitation, 1.0 mJ/pulse); positive excited state absorptive features were observed between 490 and 635 nm with wavelength maxima at 520 and 560 nm. Note that the 520 nm transient is completely superimposed with the

(59) Ghoroghchian, P. P.; Frail, P. R.; Susumu, K.; Park, T.-H.; Wu, S. P.; Uyeda, H. T.; Hammer, D. A.; Therien, M. J. *J. Am. Chem. Soc.* **2005**, *127*, 15388–15390.
(60) Susumu, K.; Frail, P. R.; Angiolillo, P. J.; Therien, M. J. *J. Am. Chem. Soc.* **2006**, *128*, 8380–8381.
(61) Duncan, T. V.; Susumu, K.; Sinks, L. E.; Therien, M. J. *J. Am. Chem. Soc.* **2006**, *128*, 9000–9001.
(62) Duncan, T. V.; Wu, S. P.; Therien, M. J. *J. Am. Chem. Soc.* **2006**, *128*, 10423–10435.
(63) Frail, P. R.; Susumu, K.; Huynh, M.; Fong, J.; Kikkawa, J. M.; Therien, M. J. *Chem. Mater.* **2007**, *19*, 6062–6064.
(64) Duncan, T. V.; Ghoroghchian, P. P.; Rubtsov, I. V.; Hammer, D. A.; Therien, M. J. *J. Am. Chem. Soc.* **2008**, *130*, 9773–9784.
(65) Fisher, J. A. N.; Susumu, K.; Therien, M. J.; Yodh, A. G. *J. Chem. Phys.* **2009**, *130*, 134506.
(66) Jung, C.; Muller, B. K.; Lamb, D. C.; Nolde, F.; Mullen, K.; Brauchle, C. *J. Am. Chem. Soc.* **2006**, *15*, 5283–5291.
(67) Métivier, R.; Nolde, F.; Müllen, K.; Basché, T. *Phys. Rev. Lett.* **2007**, *98*, 047802/1–047802/4.
(68) Melnikov, S. M.; Yeow, E. K. L.; Uji-I, H.; Cotlet, M.; Mullen, K.; De Schryver, F. C.; Enderlein, J.; Hofkens, J. *J. Phys. Chem. B* **2007**, *111*, 708–719.
(69) Kirstein, J.; Platschek, B.; Jung, C.; Brown, R.; Bein, T.; Brauchle, C. *Nat. Mater.* **2007**, 303–310.

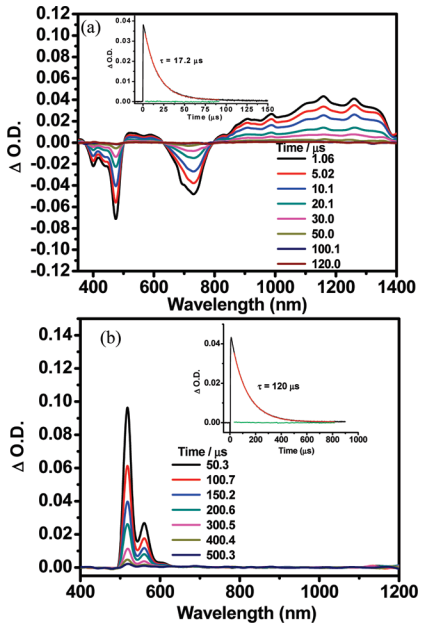


***Figure 2.*** (a) Transient absorption difference spectra of 7.0 $\mu$M **Pyr$_1$RuPZn$_2$** measured at several delay times in deaerated MTHF, 1.0 mJ/pulse, $\lambda_{ex} = 700$ nm. The inset shows the single exponential fit to the 1100 nm transient with residuals presented in green. (b) Transient absorption difference spectrum of 4.2 $\mu$M **PDI** measured at several delay times in deaerated MTHF, 1.0 mJ/pulse, $\lambda_{ex} = 485$ nm. The inset shows the single exponential fit to the 560 nm transient with residuals presented in green.

strongest ground state absorption feature as displayed in Figure 1. Analysis of the transient features observed at these wavelengths resulted in identical monoexponential decays with a time constant of 120 $\mu$s (Figure 2b). Since it is well established that **Pyr$_1$RuPZn$_2$** manifests positive excited state absorptions in the 800−1400 nm spectral region, the kinetic decay of **Pyr$_1$RuPZn$_2$** at 900 nm can be monitored exclusively as a function of increasing **PDI** concentration. Note that the triplet excited state lifetime of **Pyr$_1$RuPZn$_2$** (monitored at 900 nm) is dynamically quenched by **PDI** *via* triplet energy transfer (Figure S5). The Stern−Volmer constant and bimolecular energy transfer rate constant were readily quantified by the Stern−Volmer relation (eq 6)

$$\tau_0/\tau = 1 + K_{SV}[Q] \qquad (6)$$

where $\tau_o$ and $\tau$ are the excited state lifetimes of **Pyr$_1$RuPZn$_2$** in the absence and presence of the quencher, respectively, and [Q] is the molar concentration of the **PDI** quencher. Stern−Volmer plots of $\tau_0/\tau - 1$ versus [Q] (Figure S5) clearly demonstrate dynamic quenching with a $K_{sv}$ of 10 048 $M^{-1}$. It is important to underscore that the magnitude of $k_q$ obtained from the slope of the Stern−Volmer plot according to the relation $K_{sv} = k_q\tau_0$ corresponds to a value of $5.9 \times 10^8$ $M^{-1}$ $s^{-1}$, which is well below the diffusion limit of THF solvent ($1.3 \times 10^{10}$ $M^{-1}$ $s^{-1}$ at 20 °C).[70] In this analysis, we assume the diffusion limit of MTHF is identical to the tabulated value for THF. Similarly, dynamic quenching of the triplet excited state of **Pyr$_1$RuPZn$_2$** by dissolved dioxygen was characterized by a relatively sluggish rate constant ($1.0 \times 10^9$ $M^{-1}$ $s^{-1}$), suggesting that a weak thermodynamic driving force is only partially responsible for these results. This conclusion can be drawn based on the $^1O_2$ state energy (~0.97 eV) which adds more than 0.2 eV of driving force to the quenching process relative to **PDI**. In this latter experiment, THF was utilized as the solvent since dissolved $O_2$ concentrations in this medium are well established and no such data are available for MTHF. In both solvents, $^1O_2$ photoluminescence centered at ~1270 nm was sensitized through excitation of the supermolecular chromophore under aerated conditions; the MTHF data are presented in Figure S6. In conjunction with actinometric measurements,[46,71,72] we estimate the quantum yield for $^1O_2$ photoluminescence resulting from triplet state quenching of **Pyr$_1$RuPZn$_2$** to be on the order of 34%, which is respectable but rather low relative to other long lifetime triplet sensitizers. These data indicate that a majority of the energy transfer encounters are not producing $^1O_2$ as a product and suggest that either the low driving forces for these quenching processes, which possibly inhibit access to spin encounter species with higher potential energies, or diminished electronic coupling within donor−acceptor triplet energy transfer encounter pairs may play roles in attenuating sensitized product formation and thus limit upconversion quantum efficiencies (*vide infra*).

Upconverted fluorescence is indeed observed in these experiments and must result from sensitized triplet−triplet annihilation (TTA). Because the bimolecular rate constant obtained from the Stern−Volmer relation is almost 2 orders of magnitude lower than the diffusion rate constant of the solvent, it suggests that the driving force for triplet energy transfer from **$^3$Pyr$_1$RuPZn$_2$*** to **$^3$PDI*** is small, indicating that the energy of **$^3$Pyr$_1$RuPZn$_2$*** lies close to that of **$^3$PDI*** which has been estimated to be 1.15−1.2 eV. In an attempt to further clarify the energy of **$^3$Pyr$_1$RuPZn$_2$***, perylene was exploited as an acceptor/annihilator chromophore. A concentrated solution of perylene in MTHF was added to 3.3 $\mu$M **Pyr$_1$RuPZn$_2$**, deaerated with argon, and excited at 780 nm. No upconverted perylene fluorescence was observed under these conditions, indicating that the energy of **$^3$Pyr$_1$RuPZn$_2$*** must be lower than the triplet energy of perylene, 1.53 eV.[63] It is worthwhile to note that the singlet excited state of perylene lies at an energy where annihilation of two corresponding excited triplets ($2E_T > E_S$) is guaranteed to yield upconverted fluorescence under appropriate triplet sensitization conditions.[70] The analogous experiment utilizing tetracene as the acceptor/annihilator chromophore in MTHF does indeed display green upconverted tetracene fluorescence emission centered at 505 nm. Importantly, these data define a new anti-Stokes energy shift record for sensitized TTA photochemistry, $\Delta E = 0.86$ eV (780 nm →505 nm). The collective results of the studies above indicate that the energy of **$^3$Pyr$_1$RuPZn$_2$*** is higher than that of $^3$tetracene* (1.27 eV).[70] It therefore stands to reason that the energy of **$^3$Pyr$_1$RuPZn$_2$*** can be safely bracketed within 1.53 eV ≥ $E_T$ ≥ 1.27 eV.

Selective excitation of **Pyr$_1$RuPZn$_2$** (3.3 $\mu$M, MTHF solvent, $\lambda_{ex}$ = 780 nm) in the presence of **PDI** (420 $\mu$M) in a freeze−pump−thaw degassed solution generates upconverted **PDI** singlet fluorescence (Figure 3a). Deaerated conditions avoid the competing energy transfer reaction of **$^3$Pyr$_1$RuPZn$_2$*** with dioxygen which can substantially diminish upconversion yields in fluid solution. The integrated **PDI** upconverted fluorescence intensity measured as a function of the incident laser power was evaluated; these data were normalized to the highest

(70) Montalti, M.; Credi, A.; Prodi, A.; Gandolfi, M. T. *Handbook of Photochemistry*, 3rd ed.; CRC Press: Boca Raton, FL, 2005.
(71) Rachford, A. A.; Goeb, S.; Ziessel, R.; Castellano, F. N. *Inorg. Chem.* **2008**, *47*, 4348–4355.
(72) Rachford, A. A.; Hua, F.; Adams, C. J.; Castellano, F. N. *Dalton Trans.* **2009**, 3950–3954.

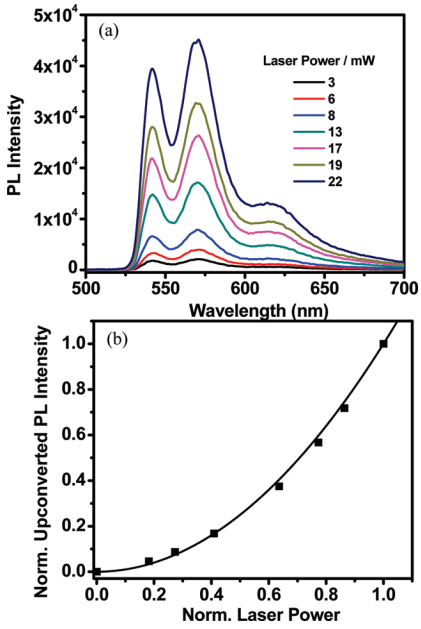


***Figure 3.*** (a) Photoluminescence intensity profile of a freeze−pump−thaw degassed MTHF solution of $\mathbf{Pyr_1RuPZn_2}$ (3.3 $\mu$M) and **PDI** (420 $\mu$M) measured as a function of 780 nm incident laser power density. (b) Normalized integrated emission intensity data from part (a) plotted as a function of the normalized incident power density of the laser. The solid black line represents the best quadratic fit to the integrated emission data.

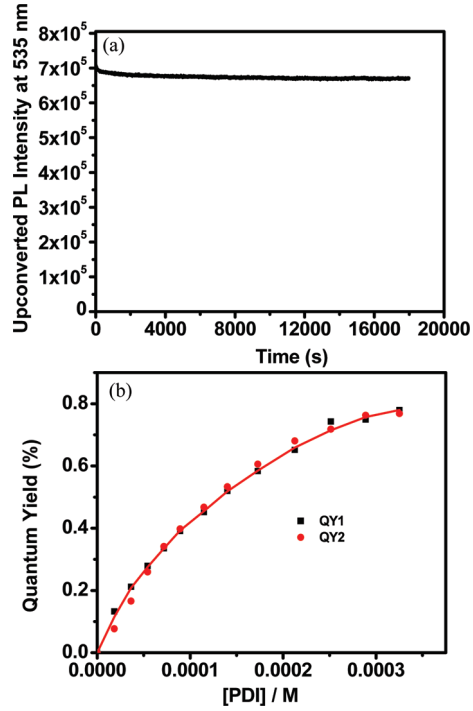


***Figure 4.*** (a) Continuous kinetic scan of the upconverted **PDI** fluorescence upon selective excitation of $\mathbf{Pyr_1RuPZn_2}$ at 780 nm at a laser power of 22 mW in a mixture of $\mathbf{Pyr_1RuPZn_2/PDI}$, $\lambda_{obs} = 541$ nm. (b) Relative percent upconversion quantum yields of $\mathbf{Pyr_1RuPZn_2/PDI}$ mixtures measured as a function of **PDI** concentration upon selective excitation of $\mathbf{Pyr_1RuPZn_2}$ at 780 nm in deaerated MTHF.

integrated emission intensity as well as to the highest incident power. Figure 3b demonstrates that the upconverted fluorescence intensity is proportional to the square of the incident excitation power over a 3−22 mW incident optical power range. The solid line in Figure 3b represents the best quadratic fit ($x^2$) to the data and establishes the nature of the nonlinear photochemistry that drives upconversion through sensitized triplet−triplet annihilation. Control experiments verified that excitation of 420 $\mu$M **PDI** at $\lambda_{ex} = 780$ nm at 22 mW resulted in no observable **PDI** fluorescence; only when both the sensitizer and acceptor are present in the same reaction mixture is **PDI** fluorescence observed upon 780 nm excitation. Figure S7 compares **PDI** fluorescence that follows 780 nm excitation and NIR triplet sensitization with the fluorescence that derives from direct $S_0 \rightarrow S_1$ excitation. Note that the sensitized fluorescence spectrum of **PDI** appears to be somewhat red-shifted (455 $cm^{-1}$) in comparison to the directly excited singlet fluorescence profile of an optical dilute solution; this effect derives from the inner filter effect caused by the high concentration of **PDI** necessary to facilitate sensitized photon upconversion. Control experiments verifying the inner filter effect as the source of this emission frequency red shift observed at high **PDI** concentrations are presented in Figure S7, thereby rendering a smaller than anticipated anti-Stokes shift (0.76 to 0.70 eV) for the sensitized TTA process. Indeed, an identical observation has been made in an all-organic upconverting composition.[21] Scheme 1 highlights the sensitizer and acceptor/annihilator energy levels, as well as the driving forces for the dynamical processes that give rise to upconverted delayed **PDI** fluorescence, and summarizes that selective excitation of $\mathbf{Pyr_1RuPZn_2}$ at 780 nm leads to TTA of **PDI**, generating $^1$**PDI***, which radiatively decays to the ground state via singlet fluorescence.

The long-term stability of this sensitizer/acceptor/annihilator system was monitored at 541 nm in an experiment that utilized continuous irradiation at 780 nm at an incident light power of 22 mW. Figure 4a indicates that the magnitude of the upconverted **PDI** fluorescence is stable over a minimum of 5 h of continuous NIR light exposure, as no obvious signs of anti-Stokes emission signal degradation are observed. Independent experiments demonstrate that $\mathbf{Pyr_1RuPZn_2}$ remains robust under identical irradiation conditions. The photochemical stability of these chromophores suggests that future device applications that take advantage of substantial anti-Stokes energy gains via a TTA process may indeed be feasible. The percent quantum efficiency of upconverted **PDI** fluorescence was measured as a function of increasing **PDI** concentration, determined relative to $[Os(phen)_3](PF_6)_2$ ($\Phi = 0.021$) in acetonitrile[40] as the quantum counter, using 680 nm excitation at a 22 mW incident power. It should be mentioned that although the emission profile of $[Os(phen)_3](PF_6)_2$ did not effectively overlap that of **PDI**, highly reproducible quantum yields were obtained over many independent measurements. Figure 4b illustrates that the upconverted **PDI** quantum efficiency increases with increasing **PDI** concentration, culminating in a $\Phi_{UC} = 0.0075 \pm 0.0002$ at the highest **PDI** concentrations utilized. Since the overall upconversion quantum efficiency is the product of the efficiencies of intersystem crossing in the sensitizer, triplet energy transfer quenching, **PDI** triplet−triplet annihilation, and singlet **PDI** fluorescence, a shortfall in one of these quantities will ultimately result in a modest upconversion quantum yield. Clearly, **PDI** singlet fluorescence will not be limiting as this value approaches unity; likewise, as it is known that the $^1\mathbf{Pyr_1RuPZn_2}^* \rightarrow {}^3\mathbf{Pyr_1RuPZn_2}^*$ intersystem crossing quantum yield nears 100% at this excitation wavelength,[29] this process does not play a role in diminishing the upconversion quantum efficiency. These facts suggest that the triplet energy transfer reaction involving $^3\mathbf{Pyr_1RuPZn_2}$ and ground-state

**PDI**, or the $^3$**PDI**-$^3$**PDI*** annihilation reaction, is responsible for the observed modest $\Phi_{UC}$ value. In this regard, note that the Stern−Volmer quenching plot of the dynamic quenching of $^3$**Pyr$_1$RuPZn$_2$*** by **PDI** shows that, at the highest acceptor/annihilator concentration available (420 $\mu$M), only 69% of the $^3$**Pyr$_1$RuPZn$_2$*** is quenched by ground state **PDI**. While this effect is congruent with the observation that the quantum yield for $^1O_2$ photoluminescence via $^3$**Pyr$_1$RuPZn$_2$*** sensitization is modest (see above), the origin of this behavior is at present obscure. Factors that may play a role in limiting the efficiency of the energy transfer process between $^3$**Pyr$_1$RuPZn$_2$*** and ground state **PDI** include (i) a low thermodynamic driving force for energy transfer (~0.22 eV) and (ii) the fact that the spatial extent of the triplet wave function of $^3$**Pyr$_1$RuPZn$_2$*** is unusually large relative to those for common triplet sensitizers.[25−32] This latter factor would be expected to give rise to low per-atom triplet excitation density in $^3$**Pyr$_1$RuPZn$_2$*** and diminished electronic coupling in **PDI** acceptor/$^3$**Pyr$_1$RuPZn$_2$*** donor energy transfer encounter complexes, relative to triplet energy transfer systems that feature electronically delocalized donors and acceptors having more compact triplet wave functions (i.e., fewer nuclei).

To gain additional perspective into what limits the upconversion quantum efficiency in the present study, the triplet−triplet annihilation rate constant ($k_{TT}$) of **PDI** in the present upconverting scheme was also determined. Knowledge of this rate constant provides insight into whether the **PDI** annihilation is diffusion limited or not. These experiments are predicated on knowledge of the molar $^3$**PDI*** extinction coefficient in MTHF solvent. This was determined through the energy transfer technique,[9,41,42] utilizing anthracene as the triplet donor and **PDI** as the acceptor. Anthracene $T_1 \rightarrow T_n$ transient absorption dynamics were monitored at 420 nm in the presence and in the absence of the acceptor, following 355 nm excitation at 1.2 mJ/pulse in argon-degassed MTHF solution (see Experimental Section), while **PDI** excited state dynamics were monitored at 560 nm. In these experiments, the **PDI** concentration was progressively increased until no further increase was observed in the 560 nm transient signal associated with $^3$**PDI***, indicating the complete triplet-state energy transfer quenching of anthracene by **PDI**. The $\Delta$OD of anthracene in the absence of the acceptor and the $\Delta$OD of the sensitized $^3$**PDI*** were taken directly from Figure S8; using these data, a previously determined $^3$anthracene* extinction coefficient ($\varepsilon_T$ anthracene at 420 nm = 42 000 $M^{-1}$ $cm^{-1}$),[41−43] and eq 5, gave the $^3$**PDI*** $T_1 \rightarrow T_n$ extinction coefficient at 560 nm [$\varepsilon_T$(560 nm) = 6.58 × $10^4$ $M^{-1}$ $cm^{-1}$]. As already presented in the Experimental Section, this wavelength was utilized since it was free of absorptive interferences; attenuation of shorter wavelength absorption by ground state bleaching transients precluded a strong case for quantitative analysis. This computed extinction at 560 nm lies in close agreement with the $T_1 \rightarrow T_n$ extinction coefficient determined previously for a closely related **PDI** derivative.[44]

With this information in hand, a concentrated solution of **PDI** (20 $\mu$M) was excited at 485 nm at high enough incident laser fluence (1.0−5.0 mJ/pulse) to facilitate annihilation of $^3$**PDI***. The $^3$**PDI*** transient absorption difference spectrum (Figure 2b) exhibits excited state absorption maxima at 520 and 560 nm. As a higher **PDI** concentration (20 $\mu$M) and a higher incident laser power (1.0−5.0 mJ/pulse) were both needed to generate a $^3$**PDI*** concentration sufficient to observe homogeneous TTA, TTA kinetics were monitored at 560 nm, instead of 520 nm, where the **PDI** ground state absorbs appreciably. Figure 5a highlights these data, which were acquired as a function of incident laser fluence at 485 nm. Analysis of these results using eq 4 gave $k_{TT}$ = (1.02 ± 0.2) × $10^9$ $M^{-1}$ $s^{-1}$, a value approximately an order of magnitude below the solvent diffusion rate constant. Figure 5b provides a representative fit (and residuals) of the transient absorption data acquired under 3.1 mJ/pulse laser fluence. Note that the measured value of $k_{TT}$ is 0.077 times that of $k_{diff}$ (in THF); this result suggests a less than optimal yield of $^1$**PDI*** from $^3$**PDI***−$^3$**PDI*** encounter pairs. While there may be a more complex origin for this behavior,[73] the **PDI** solubilizing groups may limit $^3$**PDI***−$^3$**PDI*** distances in many annihilator−annihilator encounter orientations and, thus, negatively impact $^1$**PDI*** yield. It thus appears that the substantial spatial extent of the $^3$**Pyr$_1$RuPZn$_2$*** wave function, which likely results in weak electronic coupling for energy transfers within $^3$**Pyr$_1$RuPZn$_2$***/**PDI** encounter complexes, and the nature of the **PDI** acceptor/annihilator both play roles in limiting the quantum efficiency of fluorescence upconversion via sensitized triplet−triplet annihilation.

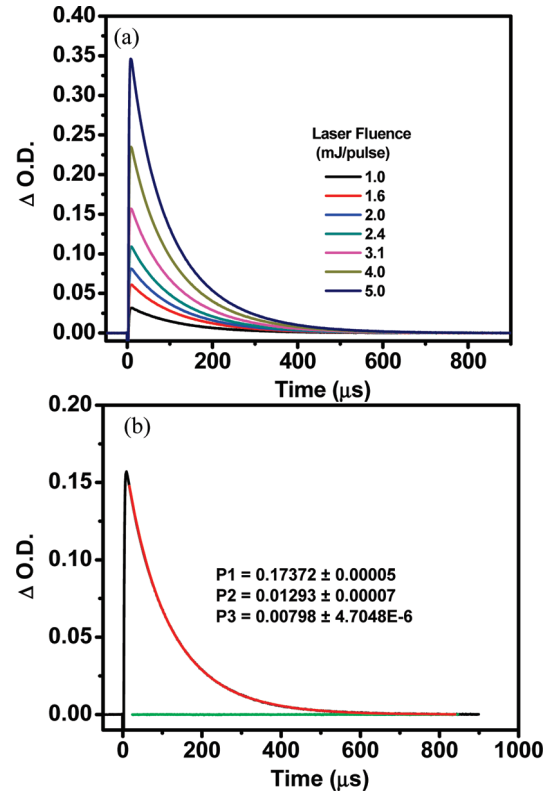


***Figure 5.*** (a) Time-resolved single wavelength absorption kinetics of **PDI** (20 $\mu$M) in deaerated MTHF monitored at 560 nm and measured as a function of incident laser pulse energy at 485 nm. (b) Representative kinetic fit (3.1 mJ/pulse) to eq 4 (red line) and the residuals of this fit (green line).

## Conclusion

Sensitized NIR-to-visible photon upconversion achieved via two sequential one photon excitations and subsequent triplet−triplet annihilation (TTA) is realized for the first time, utilizing the conjugated supermolecule **Pyr$_1$RuPZn$_2$** as the sensitizer ($\lambda_{ex}$ = 780 nm) and *N*,*N*-bis(ethylpropyl)perylene-3,4,9,10-tetracarboxylicdiimide (**PDI**; $\lambda_{em}$ = 541 nm) or

(73) Saltiel, J.; Atwater, B. W. *Adv. Photochem.* **1988**, *14*, 1–90.

tetracene ($\lambda_{em} = 505$ nm) as the acceptor/annihilator in MTHF solutions. For the experimental system utilizing the **PDI** acceptor/annihilator, we evaluate all the dynamical processes associated with this process. Selective NIR excitation (780 nm) of **$Pyr_1RuPZn_2$** in solutions containing *N*,*N*-bis(ethylpropyl)perylene-3,4,9,10-tetracarboxylicdiimide (**PDI**) gives rise to a substantial anti-Stokes energy gain of 0.7 eV, producing $^1$**PDI*** yellow fluorescence centered at 541 nm; analogous studies utilizing tetracene as the acceptor/annihilator establish a new record anti-Stokes shift of 0.86 eV for sensitized TTA. These sensitizer/acceptor/annihilator systems overcome hurdles previously associated with the realization of NIR-to-vis upconversion via triplet−triplet annihilation; these challenges have included identifying the following: (i) an NIR absorbing sensitizer having both an appreciable excited state lifetime ($\tau_T > \mu$s) and a triplet state energy appropriate for exothermic energy transfer to the visible spectral region fluorescent acceptor/annihilator and (ii) a highly soluble acceptor/annihilator chromophore with an excited state energy amenable to NIR sensitization that produces an anti-Stokes wavelength shift of sufficient magnitude to generate visible fluorescence emission. Most importantly, this particular class of supermolecular chromophore sensitizers clearly enables the utilization of newly conceived acceptors poised for device-relevant low power wavelength shifting.

**Acknowledgment.** The research conducted at BGSU was supported by the Air Force Office of Scientific Research (FA9550-05-1-0276) and the National Science Foundation (CHE-0719050). The research performed at Duke University was supported by the United States Department of Energy EFRC Program (DE-SC0001011). We thank Mr. Anthony C. Onicha (BGSU) for preparing the sample of $[Os(phen)_3](PF_6)_2$.

**Note Added after ASAP Publication.** The *x*-axis in Figure 5b was incorrect in the version published ASAP September 9, 2010. The corrected version was published September 16, 2010.

**Supporting Information Available:** Transient absorption difference spectra of anthracene in various solvents, low temperature emission spectra of **$Pyr_1RuPZn_2$**, time-correlated single-photon counting fluorescence decay data, **$Pyr_1RuPZn_2$** transient absorption difference spectra in aerated MTHF and in the presence of **PDI** in deaerated MTHF, Stern−Volmer quenching experimental data involving $^3$**$Pyr_1RuPZn_2$*** and **PDI**, prompt and delayed photoluminescence spectra of **PDI**, **$Pyr_1RuPZn_2$** sensitized singlet oxygen production, and continuous kinetic scan data of $^1$**$Pyr_1RuPZn_2$*** fluorescence in deaerated MTHF. This material is available free of charge via the Internet at http://pubs.acs.org.

JA105510K